ISSN 0021-3640, JETP Letters, 2019, Vol. 110, No. 8, pp. 562–567. © Pleiades Publishing, Inc., 2019.
Russian Text © The Author(s), 2019, published in Pis'ma v Zhurnal Eksperimental'noi i Teoreticheskoi Fiziki, 2019, Vol. 110, No. 8, pp. 557–562.

CONDENSED MATTER

Mössbauer Spectroscopy Study of $FeSe_{0.91}S_{0.09}$ Superconductor Single Crystals

K. V. Frolov[a, *], I. S. Lyubutin[a], D. A. Chareev[b, c, d], and M. Abdel-Hafiez[e, f]

[a] *Shubnikov Institute of Crystallography, Federal Research Center Crystallography and Photonics, Russian Academy of Sciences, Moscow, 119333 Russia*

[b] *Institute of Physics and Technology, Ural Federal University, Yekaterinburg, Russia*

[c] *Institute of Experimental Mineralogy, Russian Academy of Sciences, Chernogolovka, Moscow region, 142432 Russia*

[d] *Institute of Geology and Petroleum Technologies, Kazan Federal University, Kazan, 420008 Russia*

[e] *National University of Science and Technology MISIS, Moscow, 119049 Russia*

[f] *Harvard University, Cambridge, MA 02138, USA*

**e-mail: green@crys.ras.ru*

Received September 10, 2019; revised September 10, 2019; accepted September 20, 2019

Mössbauer spectra of single crystals of sulfur-doped iron selenide $FeSe_{0.91}S_{0.09}$ are studied in a wide temperature range, including the vicinity of structural and superconducting transitions. It is found that iron atoms exhibit a nonmagnetic state even in the range of helium temperatures, which can be attributed to the low-spin state of Fe^{2+} ($3d^6$, $S = 0$) ions. It is shown that this state remains nearly unchanged at temperatures close to the superconducting transition temperature. This means that the low-spin state of iron ions most probably results from some structural features and is not directly related to superconductivity. The temperature dependence of the parameters characterizing the hyperfine interaction exhibits several anomalies in the ranges of structural and electronic transitions. The Debye temperature $\Theta_M = 478$ K determined for the iron sublattice turns out to be much higher than the value $\Theta_M = 285$ K for the undoped $FeSe_{1-\delta}$ compound.

DOI: 10.1134/S0021364019200049

INTRODUCTION

The discovery of superconductivity in iron-based pnictides and chalcogenides with a relatively high transition temperature (up to 55 K) has attracted a considerable interest owing to unusual correlations between magnetism and superconductivity in these compounds [1–3]. Now, the properties of these materials are quite well studied experimentally, and several theoretical models of superconducting pairing based on magnetic fluctuations have been proposed [4–8]. The special interest in iron chalcogenides [9] is due, first of all, to the structural simplicity of these compounds, which allows treating them as convenient model systems for finding out mechanisms of superconductivity and their relation to the crystal structure and magnetic order in the iron subsystem. A new interest in iron chalcogenides is associated with FeSe based intercalated systems with T_c up to 43 K [10, 11] and with the experimental observation of superconductivity with T_c of about 80–100 K in monolayer epitaxial FeSe films deposited on a $SrTiO_3$ substrate [12–16]. The coexistence of ferromagnetism and superconductivity in FeSe crystals doped with Bi_2Se_3 was also observed [17]. Much attention is currently attracted to the studies on the interplay between the superconductivity, nematicity of the electron structure, and quantum paramagnetism in FeSe and $FeSe_{1-x}S_x$ compounds [18–25].

In this work, Mössbauer spectroscopy employing ^{57}Fe nuclei is used to study magnetic correlations in $Fe(Se_{0.91\pm0.01}S_{0.09\pm0.01})_{1-\delta}$ single crystals, as well as possible structural and electronic transformations that are expected near the superconducting transition temperature.

GROWTH OF SINGLE CRYSTALS AND THEIR CHARACTERIZATION

A batch of iron selenide layered crystals with partial substitution of sulfur for selenium $Fe(Se_{1-x}S_x)_{1-\delta}$ ($x = 0$, 0.04, 0.09, and 0.11) (Fig. 1) was grown in the shape of platelets in evacuated quartz ampules using $AlCl_3$/KCl as flux material. For 45 days, the hot and cold ends of the ampule were kept at temperatures of 400 and 350°C, respectively. The details of this technique are described in [26].

All stages of the preparation of samples for experimental studies were performed in a sealed "glove" box

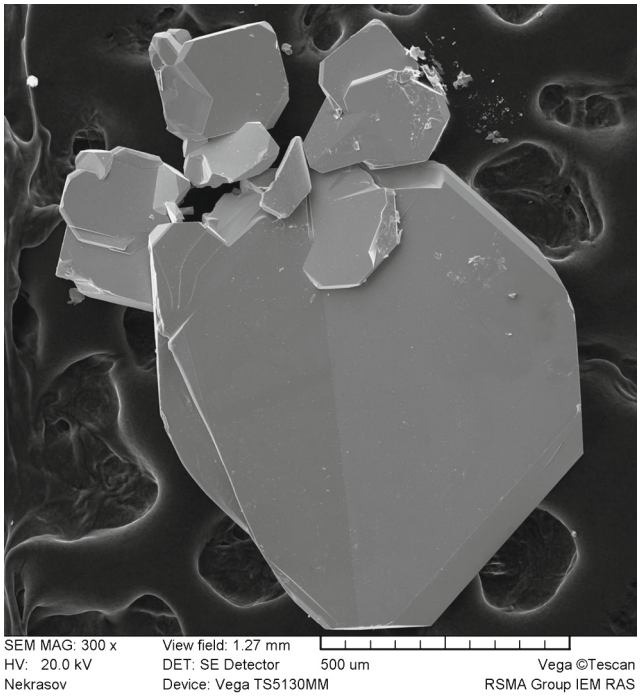

Fig. 1. Magnified image of layered platelet $Fe(Se_{1-x}S_x)_{1-\delta}$ single crystals glued on the graphite adhesive tape.

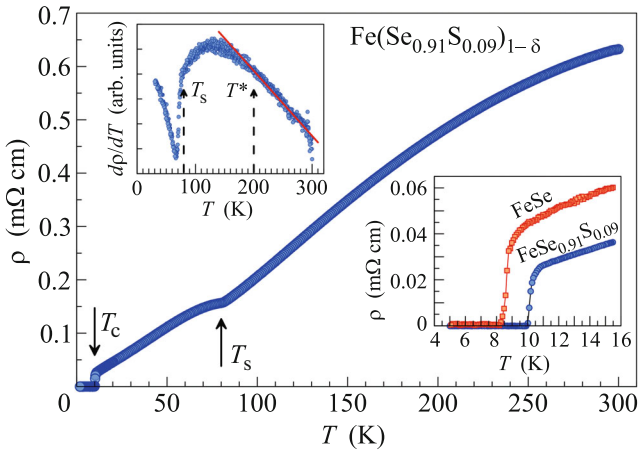

Fig. 2. (Color online) Temperature dependence of the electrical resistivity $\rho(T)$ for the $Fe(Se_{0.91}S_{0.09})_{1-\delta}$ single crystal. The lower inset shows on an enlarged scale the temperature dependence of the electrical resistivity near the superconducting transition for pure iron selenide FeSe and for the sulfur-doped $FeSe_{0.91}S_{0.09}$ crystal. The temperature dependence of the first derivative of the resistivity $d\rho/dT$ is shown in the upper inset. The arrows indicate the superconducting, structural, and nematic phase transition temperatures T_c, T_s, and T^*, respectively.

in an argon atmosphere (at O_2 and H_2O levels below 0.1 ppm). The chemical composition and structural, thermal, magnetic, and transport characteristics of $Fe(Se_{1-x}S_x)_{1-\delta}$ single crystals were analyzed. It was found that all samples contain only the β-FeSe tetragonal phase of the PbO type (the $P4/mmm$ space group). The plane of single crystal platelets coincides with the (ab) crystallographic plane.

The electrical resistivity was measured using a Quantum Design Physical Property Measurement System (PPMS) in the temperature range of 2–300 K employing the standard four-probe technique with direct current flowing in the sample plane. Electrical contacts parallel to the (ab) plane made of thin copper wires were attached to the sample with silver-containing epoxy resin. As an example, in Fig. 2, we show the temperature dependence of the resistivity $\rho(T)$ for the $Fe(Se_{0.91}S_{0.09})_{1-\delta}$ single crystal. It was found that all grown crystals are superconducting and the critical temperature T_c of the superconducting transition, critical current, and upper critical magnetic field increase with the content of the sulfur dopant ranging from 0 to 0.11 [27–29].

The Mössbauer absorption spectra for ^{57}Fe nuclei were obtained in the temperature range of 6–295 K in transmission geometry using a standard MS-1104Em Mössbauer spectrometer operating in the constant acceleration mode and equipped with specialized nitrogen and closed cycle helium [30] cryostats. The Mössbauer source $^{57}Co(Rh)$ MCo7.114 supplied by the Ritverts company [31] was used as a source of gamma rays. Isomer shifts were measured relative to the standard Mössbauer absorber α-Fe (18-μm-thick metal foil annealed in a hydrogen atmosphere). The gamma-ray source and standard absorber were kept at room temperature.

The mechanical plasticity of $Fe(Se_{1-x}S_x)_{1-\delta}$ single crystals prevents preparation of a powder by grinding them; for this reason, the absorber used in experiment is a thin continuous layer (mosaic) of overlapping single crystals. The dominant orientation of (ab) planes in the single crystals was perpendicular to the direction of the Mössbauer wave vector k_γ; i.e., gamma-ray photons propagated along the c crystallographic axis. The computer analysis of the Mössbauer spectra was performed using the Univem MS software program, contained in the software suite supplied with the spectrometer.

RESULTS AND DISCUSSION

For the Mössbauer measurements, we selected single crystals having the composition $Fe(Se_{0.91\pm0.01}S_{0.09\pm0.01})_{1-\delta}$. In Fig. 2, we show the temperature dependence of the resistivity for these single crystals. The arrows indicate the superconducting transition temperature T_c = 10.1 K and the temperature $T_s \approx 80$ K of the structural phase transition from the tetragonal phase to orthorhombic one upon cooling (see also [28]). The lower inset of Fig. 2 illustrates the data corresponding to the

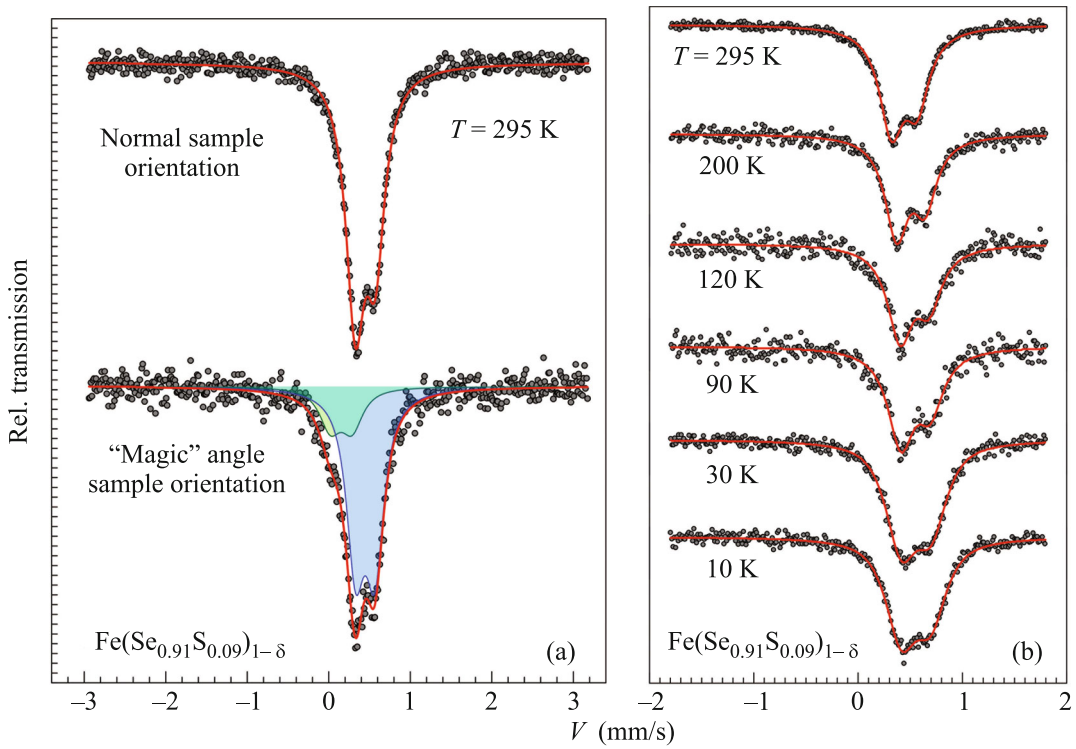

Fig. 3. (Color online) Mössbauer spectra of the superconducting $Fe(Se_{0.91}S_{0.09})_{1-\delta}$ single crystal oriented perpendicularly to the wave vector k_γ of gamma-ray photons (a, upper data) at room temperature and (b) at different temperatures. (a, lower data) Room temperature Mössbauer spectrum of the same sample oriented at the magic angle.

range of superconducting transition, which are compared to those for "pure" $FeSe_{1-\delta}$ single crystals in the absence of doping with sulfur.

In the upper inset of Fig. 2, we plot the temperature dependence of the first temperature derivative of the resistivity. An anomaly in the behavior of $d\rho/dT$ observed on cooling below temperature T^* is interpreted as a crossover from a semiconductor type behavior to a metallic one [29]. Some data [24, 29] suggest that this temperature range corresponds to the transformation of the Fermi surface, and the electron density distribution here acquires a nematic form. According to the data on the electrical resistance and the results of the Mössbauer measurements presented below, the temperature T^* for our $Fe(Se_{0.91}S_{0.09})_{1-\delta}$ crystal is about 200 K.

The Mössbauer spectra of the mosaic sample of $Fe(Se_{0.91}S_{0.09})_{1-\delta}$ crystals obtained at $T = 295$ K are shown in Fig. 3a. The presented spectra correspond to the orientation of the sample plane perpendicular to the direction of the wave vector k_γ and to the orientation at the so-called "magic" angle (54.7°), which allows eliminating the possible effect of texture on the form of the measured spectrum [32].

The spectra of the "normally" oriented sample form an asymmetric quadrupole doublet, the shape of which remains unchanged in the whole temperature range of 6.3–295 K (Fig. 3b). This type of the spectrum suggests that iron ions are in a nonmagnetic state. The spectra are well fitted at $T = 295$ K by the single asymmetric $D1$ component with an isomer shift of $\delta = 0.443(1)$ mm/s and a quadrupole splitting of $\Delta = 0.246(1)$ mm/s. These Mössbauer parameters correspond to Fe^{2+} ions in the low-spin state. In this state, all six electrons in the $3d^6$ shell of iron ions form pairs with the compensated spin (spin $S = 0$), thus leading to zero magnetic moment. Apparently, this can underlie the absence of magnetic splitting in the Mössbauer spectra at low temperatures.

Taking into account the shape and arrangement of the crystals, we suggest that the doublet asymmetry can be due to a possible deviation of the orientation of the single-crystal planes from the specified direction of the wave vector k_γ (normal to the plane). However, if the plane of the mosaic sample is rotated by the magic angle, the asymmetry of the doublet lines does not completely disappear, but the shape of the spectrum changes.

For the accurate fitting of the "magic" spectrum, it is possible to use two symmetric quadrupole doublets: $D1$ with the parameters $\delta = 0.447(4)$ mm/s and $\Delta = 0.236(9)$ mm/s, which are close to the values characteristic of the normal orientation, and $D2$ with the

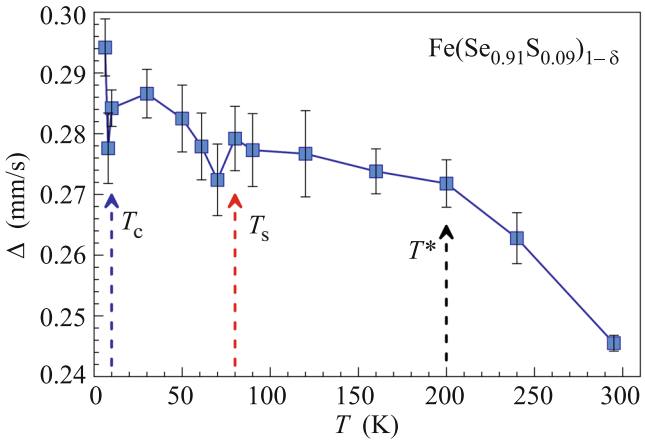

Fig. 4. (Color online) Temperature dependence of the quadrupole splitting parameter obtained from the Mössbauer spectra of the $Fe(Se_{0.91}S_{0.09})_{1-\delta}$ crystal. The solid line is a guide for the eye. The arrows indicate the superconducting, structural, and nematic phase transition temperatures T_c, T_s, and T^*, respectively.

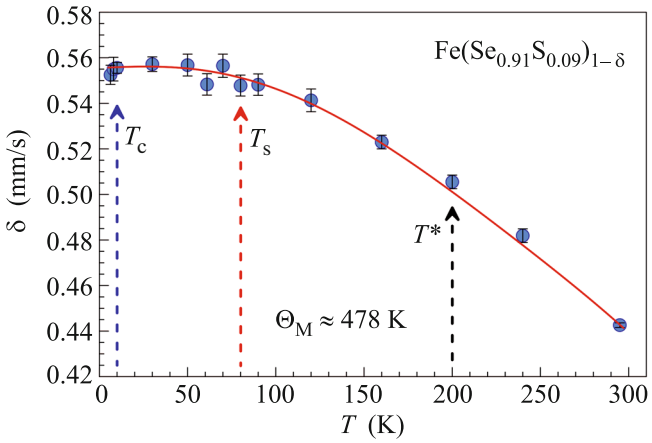

Fig. 5. (Color online) Temperature dependence of the isomer shift obtained from the Mössbauer spectra of the $Fe(Se_{0.91}S_{0.09})_{1-\delta}$ crystal. The solid line corresponds to the calculations in the second-order Doppler effect approximation. The arrows indicate the superconducting, structural, and nematic phase transition temperatures T_c, T_s, and T^*, respectively.

parameters $\delta = 0.15(3)$ mm/s and $\Delta = 0.27(4)$ mm/s. The ratio of the doublet areas is $S1 : S2 = 78 : 22$.

The $D2$ doublet seems to be associated with iron ions having a certain excess sulfur in their nearest neighborhood as compared to the sulfur content averaged over the whole volume of the crystal. The ionic radius of sulfur $R(S^{2+}) = 1.84$ Å is much smaller than that of selenium $R(Se^{2+}) = 1.98$ Å. This leads to a stronger Fe–S covalent bond, which results in a higher electron density at iron nuclei as compared to that induced by Fe–Se bonds. As a result, the isomer shift in the Mössbauer spectra for such iron atoms decreases.

The temperature dependence of the hyperfine interaction parameters $\Delta(T)$ and $\delta(T)$ obtained using the Mössbauer spectra are presented in Figs. 4 and 5, respectively.

The temperature dependence of the quadrupole splitting $\Delta(T)$ (Fig. 4) clearly exhibits a number of anomalies in the ranges of structural and electronic transitions. In particular, a kink is observed at 200 K, below which down to the structural phase transition (occurring at $T_s = 80$ K) the value of Δ increases only slightly. The temperature value $T = 200$ K agrees well with T^* characteristic of the semiconductor–metal transition deduced from the resistivity measurements (see Fig. 2).

Below the structural phase transition temperature $T_s = 80$ K, the quadrupole splitting $\Delta(T)$ exhibits an anomalous behavior, which can be related to a change in the shape of the Fermi surface (its compression) [33] in the course of the structural transformation. Near the superconducting transition temperature $T_c = 10.1$ K, a sharp jump of Δ was observed. It can result from the strong anisotropy of the superconducting gap arising owing to the electronic "nematicity" [24].

The behavior of $\delta(T)$ is characteristic of the second-order Doppler effect and does not exhibit noticeable anomalies near the phase transition temperatures T_c and T_s or near $T^* = 200$ K (all these temperatures are indicated by arrows in Fig. 5), except for slight deviations of the experimental data from the theoretical curve. The temperature behavior of the isomer shift remains nearly unchanged at the superconducting transition temperatures. This means that the low-spin state of iron ions most probably originates from structural factors and is not directly related to superconductivity. Thus, the effect of suppression of magnetism by superconductivity does not occur here. Superconductivity itself takes place if iron atoms are in the nonmagnetic low-spin state.

Using the experimentally found dependence $\delta(T)$, we determined the "Mössbauer" Debye temperature $\Theta_M = 478(1)$ K for the iron sublattice by employing the standard fitting procedure [34, 35]. Previously, the values of Θ_M were determined for the undoped $FeSe_{1-\delta}$ compound at ambient pressure, $\Theta_M = 285(4)$ K, and at the applied pressure of 6.7 GPa, $\Theta_M = 317(6)$ K [36]. It is well known that doping of $FeSe_{1-\delta}$ with sulfur leads to a compression of the unit cell induced by the so-called "chemical pressure." The effect of the latter on the physical properties can be equivalent to the application of external pressure [37, 38]. However, our value of Θ_M for $Fe(Se_{0.91}S_{0.09})_{1-\delta}$ is 160 K higher than that for the undoped $FeSe_{1-\delta}$ compound at an applied pressure of 6.7 GPa.

At the same time, the superconducting transition temperatures for $Fe(Se_{0.91}S_{0.09})_{1-\delta}$ and $FeSe_{1-\delta}$ are almost identical (T_c = 10.1 K) at ambient pressure, but the superconducting transition temperature for $FeSe_{1-\delta}$ selenide at the applied pressure exceeding 1 GPa is much higher (T_c = 34 K) [36, 39].

Note in conclusion that the problem of the temperature of formation of the nematic electronic state, which may be either higher or lower than the structural phase transition temperature T_s according to various sources, is actively discussed in the literature but is still unsolved [22, 24, 29]. Our results, including the refined T^* value, indirectly indicate that the nematic state can be formed above T_s.

FUNDING

The Mössbauer studies were supported by the Ministry of Science and Higher Education of the Russian Federation (state assignment to the Federal Research Center Crystallography and Photonics, Russian Academy of Sciences). The transport measurements were supported by the Russian Science Foundation (project no. 19-12-00414). The crystal growth tasks were supported by the Government of the Russian Federation (state contract no. 02.A03.21.0006, resolution no. 211). The work in the field of synthesis and characterization of the crystals at the Kazan Federal University was supported by the Ministry of Science and Higher Education of the Russian Federation (competitive growth program for the Kazan Federal University).

REFERENCES

1. Y. Kamihara, T. Watanabe, M. Hirano, and H. Hosono, J. Am. Chem. Soc. **130**, 3296 (2008).
2. X. H. Chen, T. Wu, G. Wu, R. H. Liu, H. Chen, and D. F. Fang, Nature (London, U.K.) **453**, 761 (2008).
3. F. C. Hsu, J. Y. Luo, K. W. Yeh, T. K. Chen, T. W. Huang, P. M. Wu, Y. C. Lee, Y. L. Huang, Y. Y. Chu, D. C. Yan, and M. K. Wu, Proc. Natl. Acad. Sci. U. S. A. **105**, 14262 (2008).
4. M. V. Sadovskii, Phys. Usp. **51**, 1201 (2008).
5. Y. Mizuguchi, Y. Hara, K. Deguchi, S. Tsuda, T. Yamaguchi, K. Takeda, H. Kotegawa, H. Tou, and Y. Takano, Supercond. Sci. Technol. **23**, 054013 (2010).
6. J. Paglione and R. L. Greene, Nat. Phys. **6**, 645 (2010).
7. V. A. Gasparov, J. Exp. Theor. Phys. **111**, 313 (2010).
8. A. A. Kordyuk, Low Temp. Phys. **38**, 888 (2012).
9. Y. Mizuguchi and Y. J. Takano, Phys. Soc. Jpn. **79**, 102001 (2010).
10. A. Zhang, T. Xia, K. Liu, W. Tong, Z. Yang, Q. Zhang, X. F. Lu, N. Z. Wang, G. H. Zhang, X. G. Luo, Z. M. Ma, B. Lei, F. Q. Huang, and X. H. Chen, Phys. Rev. B **89**, 020507(R) (2013).
11. U. Pachmayr, F. Nitsche, H. Luetkens, S. Kamusella, F. Brückner, R. Sarkar, H.-H. Klauss, and D. Johrendt, Angew. Chem. Int. Ed. **54**, 29 (2015).
12. Q. Y. Wang, Z. Li, W. H. Zhang, et al., Chin. Phys. Lett. **29**, 037402 (2012).
13. J. F. Ge, Z. L. Liu, C. Liu, C. L. Gao, D. Qian, Q. K. Xue, Y. Liu, and J. F. Jia, Nat. Mater. **14**, 285 (2015).
14. I. Bozovic and C. Ahn, Nat. Phys. **10**, 892 (2014).
15. L. Xu, Z. Lin, H. Shaolong, H. Junfeng, L. Defa, M. Daixiang, S. Bing, H. Yong, H. Jianwei, and X. J. Zhou, J. Phys.: Condens. Matter **27**, 183201 (2015).
16. M. V Sadovskii, Phys. Usp. **59**, 947 (2016).
17. Y. Liu, X. Y. Pu, K. Zhao, X. S. Yang, and Y. Zhao, Solid State Commun. **281**, 27 (2018).
18. K. K. Huynh, Y. Tanabe, T. Urata, H. Oguro, S. Heguri, K. Watanabe, and K. Tanigaki, Phys. Rev. B **90**, 144516 (2014).
19. K. Nakayama, Y. Miyata, G. N. Phan, T. Sato, Y. Tanabe, T. Urata, K. Tanigaki, and T. Takahashi, Phys. Rev. Lett. **113**, 237001 (2014).
20. R. M. Fernandes, A. V. Chubukov, and J. Schmalian, Nat. Phys. **10**, 97 (2014).
21. F. Wang, S. A. Kivelson, and D.-H. Lee, Nat. Phys. **11**, 959 (2015).
22. Q. Wang, Y. Shen, B. Pan, et al., Nat. Mater. **15**, 159 (2016).
23. Y. Sun, S. Pyon, and T. Tamegai, Phys. Rev. B **93**, 104502 (2016).
24. H. C. Xu, X. H. Niu, D. F. Xu, J. Jiang, Q. Yao, Q. Y. Chen, Q. Song, M. Abdel-Hafiez, D. A. Chareev, A. N. Vasiliev, Q. S. Wang, H. L. Wo, J. Zhao, R. Peng, and D. L. Feng, Phys. Rev. Lett. **117**, 157003 (2016).
25. P. Massat, D. Farina, I. Paul, S. Karlsson, P. Strobel, P. Toulemonde, M.-A. Measson, M. Cazayous, A. Sacuto, S. Kasahara, T. Shibauchi, Y. Matsuda, and Y. Gallais, Proc. Natl. Acad. Sci. U. S. A. **113**, 9177 (2016).
26. D. Chareev, E. Osadchii, T. Kuzmichev, J.-Y. Lin, S. Kuzmichev, O. Volkova, and A. Vasiliev, Cryst. Eng. Commun. **15**, 1989 (2013).
27. M. Abdel-Hafiez, Y. Y. Zhang, Z. Y. Cao, C. G. Duan, G. Karapetrov, V. M. Pudalov, V. A. Vlasenko, A. V. Sadakov, D. A. Knyazev, T. A. Romanova, D. A. Chareev, O. S. Volkova, A. N. Vasiliev, and X. J. Chen, Phys. Rev. B **91**, 165109 (2015).
28. S. A. Moore, J. L. Curtis, C. Di Giorgio, E. Lechner, M. Abdel-Hafiez, O. S. Volkova, A. N. Vasiliev, D. A. Chareev, G. Karapetrov, and M. Iavarone, Phys. Rev. B **92**, 235113 (2015).
29. M. Abdel-Hafiez, Y. J. Pu, J. Brisbois, R. Peng, D. L. Feng, D. A. Chareev, A. V. Silhanek, C. Krellner, A. N. Vasiliev, and X. J. Chen, Phys. Rev. B **93**, 224508 (2016).
30. P. G. Naumov, I. S. Lyubutin, K. V. Frolov, and E. I. Demikhov, Instrum. Exp. Tech. **53**, 770 (2010).
31. http://ritverc.ru/products/detail.php?ID=1112.

32. T. Ericsson and R. Wappling, J. Phys. Colloq. **37** (C6), 719 (1976).

33. M. D. Watson, T. K. Kim, A. A. Haghighirad, N. R. Davies, A. McCollam, A. Narayanan, S. F. Blake, Y. L. Chen, S. Ghannadzadeh, A. J. Schofield, M. Hoesch, C. Meingast, T. Wolf, and A. I. Coldea, Phys. Rev. B **91**, 155106 (2015).

34. *Mössbauer Spectroscopy and Transition Metal Chemistry: Fundamentals and Applications,* Ed. by P. Gutlich, E. Bill, and A. X. Trautwein (Springer, Berlin, Heidelberg, 2011), p. 81.

35. R. H. Herber, in *Chemical Mossbauer Spectroscopy,* Ed. by R. H. Herber (Plenum, New York, 1984), p. 199.

36. V. Ksenofontov, G. Wortmann, A. I. Chumakov, T. Gasi, S. Medvedev, T. M. McQueen, R. J. Cava, and C. Felser, Phys. Rev. B **81**, 184510 (2010).

37. Y. Mizuguchi, F. Tomioka, S. Tsuda, T. Yamaguchi, and Y. Takano, J. Phys. Soc. Jpn. **78**, 074712 (2009).

38. F. Sun, Z. Guo, H. Zhang, and W. Yuan, J. Alloys Compd. **700**, 43 (2017).

39. S. Medvedev, T. M. McQueen, I. A. Troyan, T. Palasyuk, M. I. Eremets, R. J. Cava, S. Naghavi, F. Casper, V. Ksenofontov, G. Wortmann, and C. Felser, Nat. Mater. **8**, 630 (2009).

Translated by K. Kugel